Absolute Photoionization Cross Section of the Ethyl Radical in the Range 8−11.5 eV: Synchrotron and Vacuum Ultraviolet Laser Measurements

ARTICLE *in* THE JOURNAL OF PHYSICAL CHEMISTRY A · MAY 2011

Impact Factor: 2.69 · DOI: 10.1021/jp202648m

THE JOURNAL OF PHYSICAL CHEMISTRY A

ARTICLE

pubs.acs.org/JPCA

Absolute Photoionization Cross Section of the Ethyl Radical in the Range 8−11.5 eV: Synchrotron and Vacuum Ultraviolet Laser Measurements

Bérenger Gans,[†] Gustavo A. Garcia,[‡] Séverine Boyé-Péronne,[†] Jean-Christophe Loison,[*,§] Stéphane Douin,[†] François Gaie-Levrel,[‡] and Dolores Gauyacq[*,†]

[†]Institut des Sciences Moléculaires d'Orsay, Université Paris-Sud 11, CNRS UMR 8214, F-91405 Orsay Cédex, France

[‡]Synchrotron SOLEIL, L'Orme des Merisiers, St Aubin, B.P. 48, F-91192 Gif-sur-Yvette Cédex, France

[§]Institut des Sciences Moléculaires, Université Bordeaux I, CNRS UMR 5255, F-33405 Talence Cédex, France

Supporting Information

ABSTRACT: The absolute photoionization cross section of C_2H_5 has been measured at 10.54 eV using vacuum ultraviolet (VUV) laser photoionization. The C_2H_5 radical was produced in situ using the rapid $C_2H_6 + F \rightarrow C_2H_5 + HF$ reaction. Its absolute photoionization cross section has been determined in two different ways: first using the $C_2H_5 + NO_2 \rightarrow C_2H_5O + NO$ reaction in a fast flow reactor, and the known absolute photoionization cross section of NO. In a second experiment, it has been measured relative to the known absolute photoionization cross section of CH_3 as a reference by using the $CH_4 + F \rightarrow CH_3 + HF$ and $C_2H_6 + F \rightarrow C_2H_5 + HF$ reactions successively. Both methods gave similar results, the second one being more precise and yielding the value: $\sigma_{C_2H5}^{ion}$ = (5.6 ± 1.4) Mb at 10.54 eV. This value is used to calibrate on an absolute scale the photoionization curve of C_2H_5 produced in a pyrolytic source from the $C_2H_5NO_2$ precursor, and ionized by the VUV beam of the DESIRS beamline at SOLEIL synchrotron facility. In this latter experiment, a recently developed ion imaging technique is used to discriminate the direct photoionization process from dissociative ionization contributions to the $C_2H_5^+$ signal. The imaging technique applied on the photoelectron signal also allows a slow photoelectron spectrum with a 40 meV resolution to be extracted, indicating that photoionization around the adiabatic ionization threshold involves a complex vibrational overlap between the neutral and cationic ground states, as was previously observed in the literature. Comparison with earlier photoionization studies, in particular with the photoionization yield recorded by Ruscic et al.[1] is also discussed.

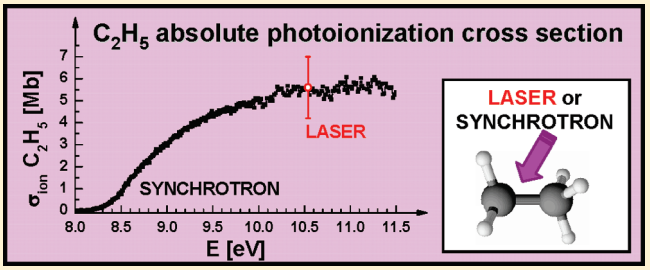

I. INTRODUCTION

Hydrocarbon radicals and their cations play an important role in the carbon chemistry of the interstellar space[2,3] and in combustion.[4,5] In particular, cations of the hydrocarbon radicals are involved in the gas-phase reactivity leading to the formation of larger organic molecules. In the modeling of complex photochemical reaction chains, important data concern the photoionization cross section of these very reactive species. Furthermore, in laboratory experiments, photoionization mass spectrometry is often used as a diagnostic tool but it requires the knowledge of the absolute photoionization cross sections in order to perform quantitative studies. While absolute photoionization cross sections are available for many stable hydrocarbons, they are still very scarce for radical hydrocarbons[6−10] since both the production stage and the concentration determination are challenging issues.

Ethyl radical and its cation not only are fundamental species in interstellar space but they also frequently appear in laboratory mass spectra of many hydrocarbon molecules.[11] A considerable amount of theoretical and experimental work has been devoted to the photoionization of this radical. The experimental adiabatic ionization energy, measured either by photoelectron spectroscopy[12,13] or by photoionization mass spectrometry,[1,5,14] exhibits large variations, from 8.117 to 8.38 eV. The difficulty of this determination is essentially due to a large change in geometry between the neutral and the cationic species. Indeed, in the neutral and cationic species, ab initio calculations predict three geometrical structures: two C_s classical structures $CH_2−CH_3$ with low barriers to internal CH_3 rotation but a high barrier for hydrogen atom scrambling, and one nonclassical singly bridged structure in which one of the H atoms is located above the CC bond.[1] In the neutral, one classical structure is the most stable whereas the bridged nonclassical structure is about 2 eV higher in energy.[1] In the cation, unlike the neutral, the bridged classical structure corresponds to the only minimum on the ground state potential

Received: March 21, 2011
Revised: April 19, 2011
Published: May 06, 2011

energy surface (see refs 15 and 16 and references therein), with nevertheless a very small calculated barrier for proton scrambling connecting the nonclassical (ground state) geometry to the classical (transition state) structure. As shown by the PFI-ZEKE (pulsed field ionization zero kinetic energy photoelectron) spectrum[17] as well as the measured photoionization signal,[17,18] the gradual onset on the photoionization signal indicates a large change of geometry upon ionization and very small Franck−Condon factors at threshold. Large amplitude motions accompanied by rapid exchange of the protons are expected to be dominant in the cation and could explain the dense and complex structure observed in the photoelectron spectrum.[13] In addition to this very complicated vibrational structure at the onset of ionization, the internal energy carried by the ethyl radical has a large impact on the shape of both photoelectron spectra[13] (PES) and photoionization spectra.[1] Dyke et al. observed a broad unstructured PES band when ethyl was formed by pyrolysis of azoethane, while a cleaner and structured band appeared in their PES when ethyl radical was formed by the abstraction reaction of F atoms with C_2H_6, exhibiting internal energies characteristic of room temperature.[13] This spectral difference was later rationalized by the calculations of Ruscic et al.[1] The internal energy dependence of the relative photoionization yield of C_2H_5 has later been studied by Fan and Pratt, who recorded ion images, for a fixed wavelength of the vacuum ultraviolet (VUV) ionization laser, of ethyl formed by 266 nm photodissociation of ethyl iodide.[19] Despite all the above theoretical and experimental efforts focused on the photoionization of ethyl radical, the photoionization cross section of ethyl has never been measured with an absolute scale over an extended range until now, especially around the adiabatic threshold 8.117 eV.[1] The only absolute measurement to date has been done recently by FitzPatrick et al.[8] yielding a cross section value of 8 ± 2 Mb at the fixed photon energy of 13.8 eV.

The goal of this work is to obtain the photoionization cross section of C_2H_5 on an absolute scale from 8 to 11.5 eV. This has been done in two steps by using two experimental setups associated with two radiation sources and different radical productions. By using the synchrotron radiation and a radical pyrolysis source, the photoionization yield has been measured on the desired range. The direct photoionization yield has been obtained and discriminated from other ionization processes such as dissociative ionization thanks to a careful ion image treatment of our data. This curve has been plotted on an absolute scale thanks to VUV laser data recorded with a radical source based on the $F + C_2H_6$ reaction. This new result is finally discussed and compared with previous data from the literature.

II. EXPERIMENTAL SECTION

The present experiments have been carried out with two independent experimental setups, by using a synchrotron radiation based electron/ion coincidence spectrometer coupled to a pyrolysis source and a laser-based mass spectrometer coupled to a gas phase reactor chamber.

A. Synchrotron Photoionization Measurements. A pure liquid sample of nitroethane, $C_2H_5NO_2$ (Sigma-Aldrich, 98% purity, stabilized in ethanol), was placed into a bubbler at room temperature. A gentle flow of Ar at a pressure of 0.5 bar was used to expand the resulting vapor through a 50 μm nozzle. Immediately after the supersonic expansion, the precursor gas entered a flash pyrolysis reactor described elsewhere[10] consisting of a resistively heated SiC tube, with a pyrolysis power of about 35 W. The formed C_2H_5 radicals and the other products of the pyrolysis passed through a 0.7 mm skimmer and entered the ionization chamber of the DELICIOUS II spectrometer[20] where they crossed the VUV photon beam at a right angle. The electrons and ions produced were then accelerated in opposite directions by the constant extraction field inside the spectrometer. They were detected in coincidence by means of velocity map imaging (VMI) and a Wiley−McLaren time-of-flight (TOF) mass spectrometer, for the electrons and the ions, respectively. The extraction field was fixed at 381 V/cm to ensure that all the electrons with kinetic energies below 3.8 eV were collected.

In the coincidence operation mode, the spectrometer was capable of recording not only TOF spectra but also mass-selected photoelectron images. With change of the polarity of the electrodes, the detection scheme could be easily inverted, so that mass-selected ion images of the pyrolysis products could be recorded to determine translational energies for all the detected masses. We will see in the following section that this type of experiment is useful for photon energies above the onset of dissociative photoionization of the precursor.

The VUV photons were delivered by the DESIRS beamline,[21] located at the SOLEIL French synchrotron facility. This undulator-based beamline is equipped with a 6.65 m normal incidence monochromator fitted with four spherical gratings covering the 5−40 eV energy range. For the present work the 200 grooves/mm grating was chosen, providing a moderate energy resolution with a high photon flux. The monochromator slits were set to give an energy resolution of 17 meV at 10.0 eV. Argon was introduced at a pressure of 0.26 bar into a windowless gas filter[22] located upstream the monochromator, in order to efficiently cut off the higher harmonics produced by the undulator and achieve a high spectral purity at the sample level. The photon flux of the beamline was measured continuously by a photodiode (AXUV100, IRD) placed after the ionization chamber, so that all the data presented in this work have been corrected by the photon flux.

B. VUV Laser Measurements. The experimental setup used in the laser study has been detailed elsewhere[23] It consists of a fast flow reactor coupled to a TOF mass spectrometer (D850 Reflectron Jordan Co.,USA). The C_2H_5 radicals were produced from the following reaction

$$C_2H_6 + F \rightarrow C_2H_5 + HF \quad (1)$$

The F atoms were formed by a microwave discharge at 2450 MHz (Sairem GMP 03 KSM) in a mixture of 1% F_2 in He (Linde), introduced into the 24 mm main reactor 50 cm upstream from the reaction zone. Using electron beam ionization, we checked that 100% of the F_2 molecules were dissociated leading to a typical F atom initial concentration in the flow tube ranging from 1 to 10×10^{12} molecules·cm^{-3}. Methane (Linde 5.5) or ethane (Linde 4.0) were premixed in a secondary flow of He gas in large excess with respect to the F concentration (typically $[CH_4]$ or $[C_2H_6] = (1-10) \times 10^{14}$ molecules·cm^{-3}) and were introduced through a second medium tube (12 mm). NO_2 gas (1% in He, AlphaGaz; typically $[NO_2] = 1 \times 10^{14}$ molecules·cm^{-3}) was premixed in a third flow of He gas and was introduced through the injector (tube of 6 mm with showerhead mixer) to induce the second reaction

$$C_2H_5 + NO_2 \rightarrow C_2H_5O + NO \quad (2)$$

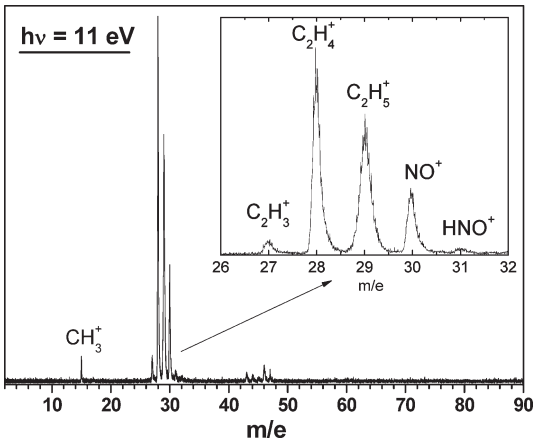

Figure 1. Time-of-flight mass spectrum obtained at the SOLEIL synchrotron facility at 11 eV from the pyrolysis of $C_2H_5NO_2$ (35 W pyrolysis power). The inset shows the region m/e = 26−32 on an enlarged scale.

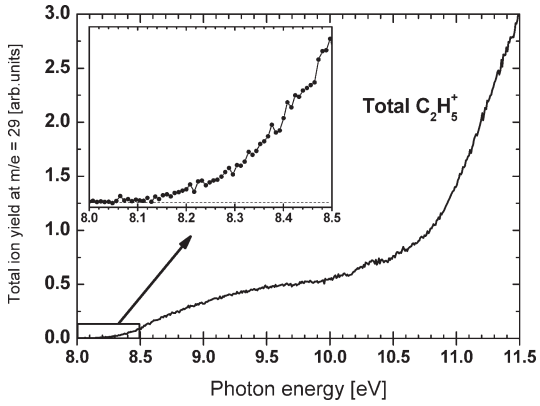

Figure 2. Total photoionization yield of the ethyl radical (m/e = 29) recorded at the synchrotron facility with a 8 meV step, including all ionization processes before imaging deconvolution. The inset shows the region of the first onset of the signal on an enlarged scale between 8 and 8.5 eV.

The flow in the injector was kept constant for the experiment with and without NO_2, by adjusting the helium flow, to ensure constant flow conditions in the reactor. Gas flow rates were measured with carefully calibrated Tylan FC-2900 mass flow controllers. Typical flow velocities ranged from 14 to 31 $m \cdot s^{-1}$.

Reaction 1 was induced before injection of NO_2 not only to avoid the cross reaction between F atoms and NO_2 but also to ensure that C_2H_5 radicals are thermalized to ambient temperature before reacting with NO_2. By comparison with the F + CH_4 → HF + CH_3 reaction[24] we can assume that the excess energy of the F + C_2H_6 → HF + C_2H_5 reaction (ΔH = −34.8 kcal/mol)[25] is mainly localized in the HF vibration. In our conditions of first-order kinetics with CH_4 or C_2H_6 introduced in large excess, we can neglect secondary reactions between the F atom and CH_3 or C_2H_5 radicals.

The reactor zone is connected to the mass spectrometer via a differentially pumped orifice-skimmer chamber. The reacting gases at 0.6−2 Torr total pressure were expanded through a 1.0 mm diameter homemade Kel-F skimmer[26] into a region where the background pressure was maintained at 1 mTorr. The centerline portion of the expanded jet passed through a 2.1 mm skimmer aperture (Beam Dynamics) into the ionization chamber, which was maintained at less than 10^{-5} Torr. Ionized particles were extracted and sent to the detector through a 820 mm reflectron (mass resolution $R_{50\%}$ of 1200 at m/e = 30), maintained at 10^{-7} Torr. Ions were detected through microchannel plate detectors, and the corresponding signals were acquired by a digital oscilloscope and sent to a microcomputer.

The mass discrimination factor for equivalent experimental pressure and flow conditions has been determined in a previous study.[9]

The photons (117.6 nm (10.54 eV) and 118.3 nm (10.48 eV)) used in this study were generated by tripling a UV laser beam (352.8 and 354.9 nm) in a rare gas (30 Torr of Xe) filling up a quartz cell equipped with an entrance quartz window and a MgF_2 lens as exit window. The UV beam was focused with a quartz lens (f = 150 mm) before entering the tripling cell. The VUV beam was focused through the MgF_2 lens in the ionization region, 120 cm downstream, while the UV beam was widely dispersed by the same lens, in order to avoid multiphoton ionization processes with the UV beam. This was checked by pumping the tripling medium, leading to a complete disappearance of the ion signal.

III. RESULTS AND DISCUSSION

A. Synchrotron Experiments. Figure 1 shows a typical TOF mass spectrum recorded by using the pyrolysis of the $C_2H_5NO_2$ precursor for a pyrolysis power of 35 W and at a photon energy of 11 eV. In these conditions, several masses appear in the mass spectrum, with the most intense corresponding to $C_2H_4^+$, $C_2H_5^+$ NO^+, and H_2CO^+, all of them produced in the flash pyrolysis reactor from $C_2H_5NO_2$. Note that the precursor mass peak (m/e = 75) is not seen either in the mass spectrum of Figure 1 or when the pyrolysis source is turned off, due to the unstable character of the ground state cation which directly dissociates to give $C_2H_5^+$.

In addition, weaker mass signals are observed at m/e = 15, 27, 31, 43, 44, 45, 46, and 47 amu. They are produced either as byproducts of the $C_2H_5NO_2$ pyrolysis (like C_2H_3, HNO, C_2H_4O, and HNO_2) or by photoionization and dissociative ionization of known impurities such as ethanol (present in the $C_2H_5NO_2$ sample as stabilizer) or acetone, leading to CH_3^+, CH_3CO^+, $C_2H_5O^+$, and $C_2H_5OH^+$.

The total ion yield (TIY) recorded at m/e = 29 and corresponding to the ethyl radical has been measured as a function of the photon energy, in the 8−11.5 eV energy range. The result is shown in Figure 2. The curve presents two regions: (i) a very smooth onset above 8.12 eV (see the inset of Figure 2); (ii) a sudden increase marked by a change of slope around 10.8 eV. The ionization energy (IE) of the precursor is very close to this value (10.9 eV), and the $C_2H_5NO_2^+$ cation is expected to dissociate in its ground state to give $C_2H_5^+$ as mentioned above. Thus the second onset is readily assigned to the dissociative ionization of the precursor, while the first one corresponds to direct ionization of the ethyl radical produced by pyrolysis of $C_2H_5NO_2$.

The two processes leading to the formation of the $C_2H_5^+$ cation are described in eqs 3 and 4 below:

direct ionization of hot neutral C_2H_5

$$C_2H_5NO_2 \xrightarrow{T} C_2H_5 + NO_2 \xrightarrow{h\nu} C_2H_5^+ + NO_2 \qquad (3)$$

dx.doi.org/10.1021/jp202648m |J. Phys. Chem. A 2011, 115, 5387–5396

dissociative ionization of $C_2H_5NO_2$

$$C_2H_5NO_2 \xrightarrow{h\nu} C_2H_5^+ + NO_2 \qquad (4)$$

They correspond to direct ionization of C_2H_5 after the pyrolysis process (eq 3) and to dissociative ionization of the precursor $C_2H_5NO_2$ (eq 4), respectively. Since we expect some translational energy to be deposited into the fragments in the case of dissociative ionization, the two processes can be discriminated by determining the kinetic energy associated to the $C_2H_5^+$ mass as measured by the velocity map imaging technique.

As mentioned in the Experimental Section, inverting the polarity of the electrodes allows the recording of mass selected ion images. Panels a and b of Figure 3 show $C_2H_5^+$ ion images recorded at 9.5 and 11.5 eV, respectively. At 9.5 eV (Figure 3a), only the direct ionization of the ethyl radical should be present, and indeed the ion image shows the typical footprint of the molecular beam, with a velocity vector distribution along the molecular beam axis. At 11.5 eV (Figure 3b) the image exhibits an additional halo, corresponding to ions with larger kinetic energies and isotropic distribution, typical of a dissociative process in the ion precursor. Both the direct and dissociative contributions can be extracted as shown in panels c and d of Figure 3: the transverse projection of the image can be fitted by two Gaussian curves related to the two different events. The areas of the Gaussian fits represent the contribution of each process. The dissociative ionization clearly appears through the red area in Figure 3d.

We have applied this deconvolution procedure for mass selected ion images recorded every 16 meV within the 9.5−11.5 eV energy range, and the results are plotted in Figure 4 for the $C_2H_5^+$ ion. From the dissociative ionization curve depicted in Figure 4b), we determine the appearance energy (AE) of $C_2H_5^+$ from $C_2H_5NO_2$ as 10.85 ± 0.05 eV by linear

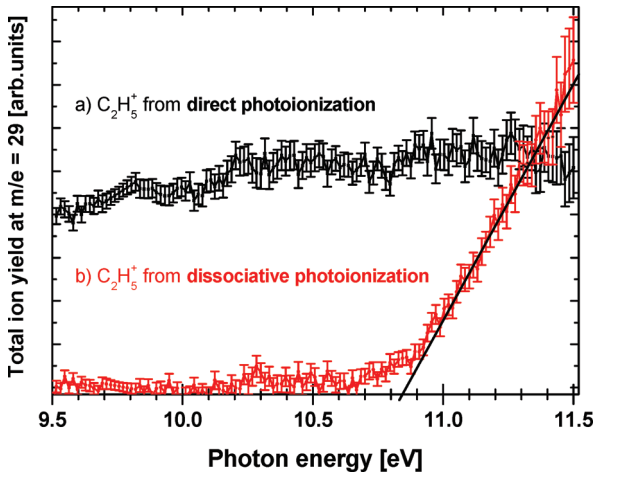

Figure 4. Partial ion yields for ethyl radical between 9.5 and 11.5 eV (16 meV step) obtained by applying the deconvolution procedure to the $C_2H_5^+$ ion images (see text for details): (a) direct photoionization of C_2H_5 (black dots) and (b) dissociative photoionization of $C_2H_5NO_2$ (red dots).

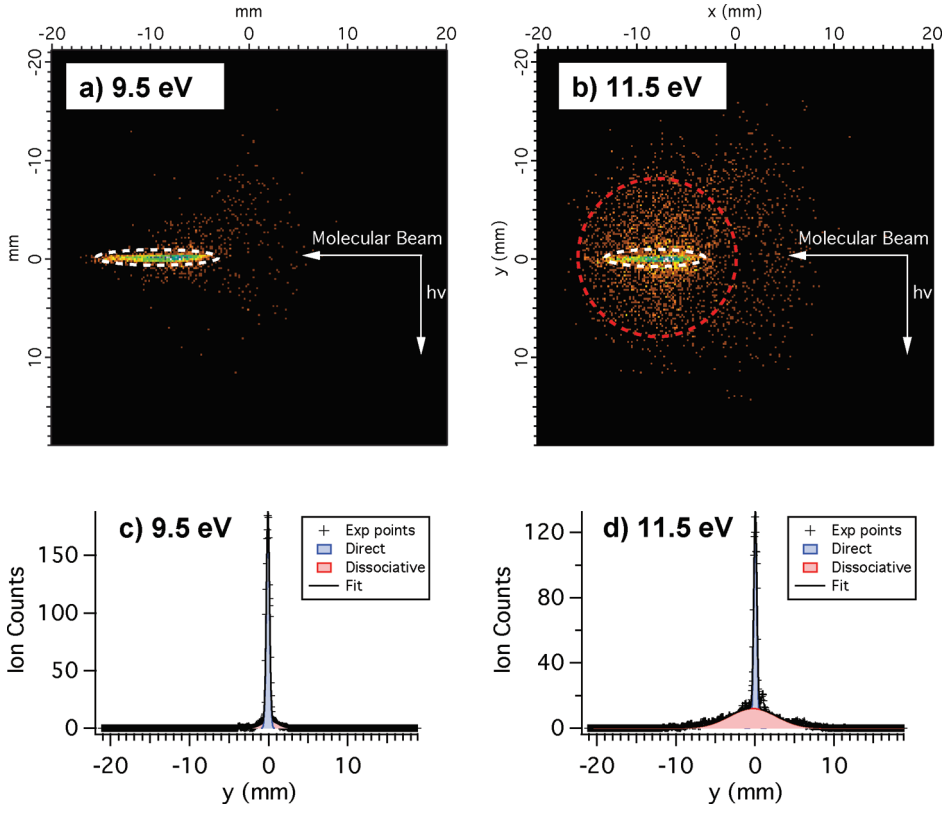

Figure 3. $C_2H_5^+$ velocity map ion images recorded at (a) 9.5 and (b) 11.5 eV with an extraction field of 95 V/cm. The white dashed line encircles the position of the "cold ions" formed by direct ionization, while the "hot ions" with bigger kinetic energies yield spots contained within the red dashed circle. The transverse projections of the images explaining the deconvolution procedure are plotted in the lower panels at (c) 9.5 and (d) 11.5 eV. Two Gaussian functions are used to model the projections, representing the cold (blue area) and the hot (red area) contributions to the total fit (black line).

dx.doi.org/10.1021/jp202648m |J. Phys. Chem. A 2011, 115, 5387–5396

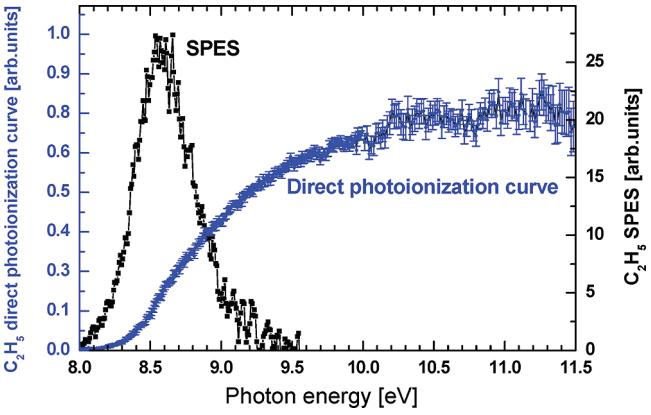

Figure 5. Direct C_2H_5 ion yield (blue solid line) and slow photoelectron spectrum (SPES, black circle) of the ethyl radical. The SPES was obtained by integrating electrons with kinetic energies in the range 0−300 meV. A "folding" procedure of the 2D matrix of intensities as a function of both the electron kinetic energy and the photon energy is applied, as explained in the text and in ref 29, and yields a moderate resolution of 40 meV over the photon energy range (8−9.5 eV) for the SPES.

extrapolation of the onset. This measured AE is very close to the IE of $C_2H_5NO_2$ (10.9 eV) and in reasonable agreement with the electron impact value[27] (11 eV). However, a weak ion signal is discernible already from 10.7 eV, and we assign this signal to hot band transitions due to the heating of the neutral $C_2H_5NO_2$ molecules in the pyrolysis tube.

The ion imaging and the PEPICO experiments allow then the direct total ion yield of the ethyl radical to be plotted in the 8.0−11.5 eV energy range, after eliminating the precursor's dissociative channel. This direct photoionization yield is displayed in Figure 5. This curve exhibits a smooth increase from the ionization threshold and reaches a plateau around 10.5 eV.

Another advantage of the imaging spectrometer used in this work is that at each point of the scan presented in Figure 2, we obtain not only a TOF spectrum but also a photoelectron image for all the masses present in the TOF. These images can be Abel inverted[28] to extract the PES. Thus, for any given mass we are able to obtain a 2D matrix of intensities as a function of both the electron kinetic energy and the photon energy. The information contained in this matrix powerfully probes the ionization mechanisms via the measurement of the so-called "slow photoelectron spectrum" (SPES), as has been recently demonstrated.[29] Briefly, the 2D matrix is folded so that the coincidence ion-electron signals (corresponding to given ionic states) are parallel to the kinetic energy axis. The electron counts are then integrated from 0 to some small value (typically tens of millielectronvolts), representing the best compromise between signal-to-noise ratio and resolution, at each photon energy to build the SPES.[29]

The SPES of the ethyl radical obtained in this manner is shown in Figure 5 together with the direct photoionization ion yield. It exhibits a broad band centered around 8.55 eV extending from 8 to nearly 9.5 eV which can be assigned to an extensive overlap of long and unresolved vibrational progressions, in agreement with the significant change of geometry upon ionization calculated by Ruscic et al.[1] In their calculations, the neutral ethyl radical shows a minimum energy at a classical structure with nearly free rotation of the methyl group around the CC bond, and the ethyl cation shows an equilibrium structure with a bridged nonclassical structure. Therefore one can expect several vibrational progressions to

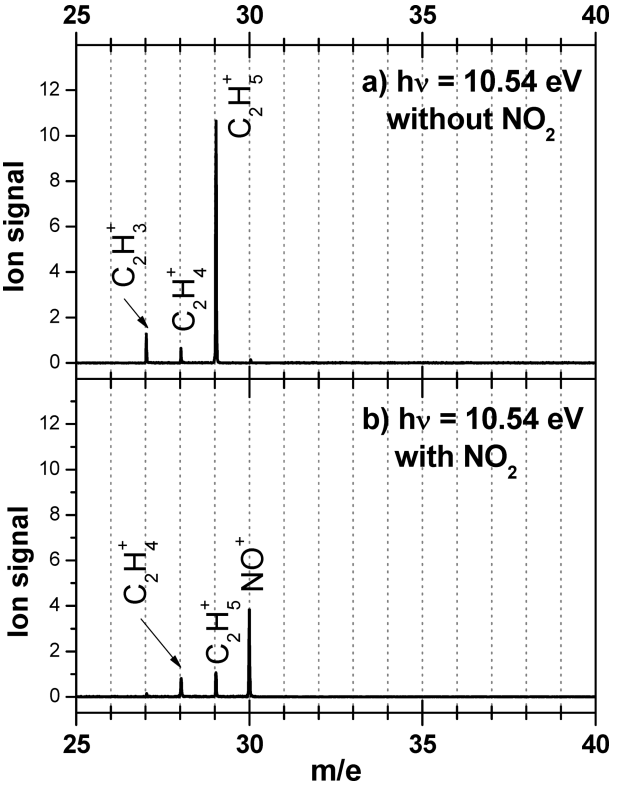

Figure 6. Mass spectra recorded in the laser experiment at 10.54 eV for the C_2H_5 radical produced by reactivity with fluorine atoms: (a) without introduction of NO_2 in the flow reactor, and (b) in the presence of NO_2.

be observed upon ionization, as was suggested by Ruscic et al.[1] These authors confirmed the Dyke et al.[13] conclusions on their PES spectra pointing out that the different vibrational populations in their PES were related to the production source of the radical (either pyrolysis or reactive production).

The onset region of the ionization curve has been examined in detail by Willitsch et al.[17] and Schussler et al.[18] Willitsch et al.[17] presented a PFI-ZEKE spectrum in the region 8.22−8.46 eV showing a rich vibrational structure. Schussler et al.[18] showed a photoionization efficiency curve in the region 8.0−8.8 eV indicating a small signal around 8.12 eV in agreement with the value reported by Ruscic et al.

B. Absolute Measurement of the Photoionization Cross Section of C_2H_5 at Fixed Photon Energies (10.48 and 10.54 eV). The first way to measure the absolute photoionization cross section of the C_2H_5 radical is to induce reactions 1 and 2 described in section II.B and to simulate the kinetics of reaction 2 by recording the ratio of C_2H_5 depletion and NO appearance as a function of time. It should be noted that C_2H_5O was never detected likely due to two effects: (i) its photoionization cross section is very low below 10.78 eV,[30] (ii) it reacts with NO_2 leading mainly to $C_2H_5ONO_2$ ($k = 2.8 \times 10^{-11}$ cm^3·molecule^{-1}·s^{-1})[31] which is most likely undetectable with our VUV photon energies (by comparison with the IE of CH_3ONO_2, 11.53 eV[32]).

Typical VUV (10.54 eV) mass spectra of the C_2H_5 radical obtained in the laser experiment are shown with the same relative scale without and with NO_2, in Figure 6a) (reaction 1 only) and Figure 6b) (reaction 1 + reaction 2), respectively.

In Figure 6a, aside from the $C_2H_5^+$ signal, weaker signals appear at the masses of $C_2H_3^+$ and $C_2H_4^+$. The $C_2H_4^+$ ion peak

dx.doi.org/10.1021/jp202648m |J. Phys. Chem. A 2011, 115, 5387–5396

comes from C_2H_4 impurities present in the C_2H_6 cylinder (measured at 0.04% relative to C_2H_6 using known allene concentration as a reference) and from the $C_2H_5 + C_2H_5 \rightarrow C_2H_4 + C_2H_6$ reaction (this point is discussed later in the text). The $C_2H_3^+$ signal intensity is about 8% of that of $C_2H_5^+$ and is being discussed in the following.

In this laser experiment, we have to verify that the $C_2H_5^+$ and NO^+ signals appearing in panels a and b of Figure 6 do not involve a two-photon mechanism, either (VUV + VUV) or (VUV + UV). We have found that the signal ratio $C_2H_5^+/NO^+$ following reaction 2 ($C_2H_5 + NO_2 \rightarrow C_2H_5O + NO$) is constant for various VUV and UV beam intensities, and VUV focusing conditions, at 10.48 and 10.54 eV. If two-photon mechanisms leading to $C_2H_5^+$ and NO^+ ions occurred, they should not lead to a constant ratio. Hence multiphoton mechanisms can be neglected for the production of $C_2H_5^+$ and NO^+, and the $C_2H_5^+$ signal is proportional to the VUV laser intensity.

If we now consider the $C_2H_3^+$ signal observed in Figure 6, two possible processes can be invoked: (i) dissociative ionization of C_2H_5; (ii) ionization from neutral C_2H_3 produced in the reactor.

Process i, dissociative ionization of C_2H_5 into $C_2H_3^+ + H_2$, has been observed in synchrotron experiments by Schussler et al.[18] above the one-photon energy of 11.5 eV. This appearance energy is well above the calculated value of 10.42 eV, taking into account an energy barrier of 0.1 eV for dissociative ionization.[33,34] Therefore the $C_2H_3^+$ ions should not come from dissociative ionization induced by one VUV photon only but rather from a concerted (VUV + UV) dissociative photoionization mechanism or from a (VUV + VUV) process. By variation of the UV beam intensity, as well as the VUV focusing conditions, the signal ratio $C_2H_3^+/C_2H_5^+$ was revealed to be constant, implying that the $C_2H_3^+$ signal cannot be explained by a two-photon (either VUV + VUV or VUV + UV) mechanism since the $C_2H_5^+$ signal is proportional to the VUV photon flux. Therefore dissociative ionization of C_2H_5 can be ruled out.

Then process ii must be invoked for the observation of the $C_2H_3^+$ signal (8% of the $C_2H_5^+$ signal) involving the formation of neutral C_2H_3 radical in the reactor prior to ionization. At this stage, we did not find a simple and plausible reaction for this production since no reaction with fluorine exists (no $C_2H_3F^+$ signal is observed for instance, even though its IE is 10.36 eV[35]). If the reactions responsible for the C_2H_3 formation involved C_2H_5, they could affect the C_2H_5 initial concentration to some extent and consequently the value of the measured photoionization cross section. On the other hand, the photoionization cross section of C_2H_3 has been measured by Robinson et al.[6] to be about 14 Mb at 10.5 eV, which is significantly larger than the expected value for C_2H_5 determined below (5.6 Mb). Therefore the maximum incidence of the C_2H_3 formation on the C_2H_5 photoionization cross section has been taken into account in the present work by increasing the error bar by 3%.

If we now go back to the key reaction 2, the typical kinetics of the C_2H_5 disappearance and NO appearance are shown in Figure 7 together with their corresponding simulation. The area of the ion peak signal of a species X, S_X, is given by the equation

$$S_X(t) = \eta(t) F_X \sigma_X^{ionVUV} [X(t)] \qquad (5)$$

where $\eta(t)$ is the apparatus function factor which includes the real-time intensity of the VUV beam, F_X is the mass discrimination factor, σ_X^{ionVUV} is the absolute photoionization cross section at the VUV wavelength, and $[X(t)]$ is the concentration which

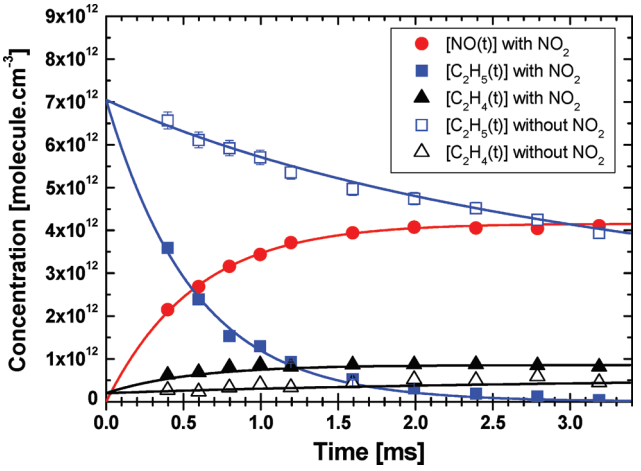

Figure 7. Typical kinetics of C_2H_5 disappearance and NO appearance with their respective simulations: experimental points are shown by circles for $[NO(t)]$, squares for $[C_2H_5(t)]$, and triangles for $[C_2H_4(t)]$. Open symbols represent experimental concentrations without NO_2 in the reactor; full symbols represent experimental concentrations when NO_2 is added in excess in the reactor. The solid lines represent the simulated concentrations with the kinetic model based on the reactions of Table 1. The relation between mass signals S_X and concentrations [X], with respect to NO, is detailed in the text.

depends on the kinetic model associated to all reactions occurring in the reactor and presented in Table 1. The apparatus function factor is determined for each scan by fitting the NO^+ signal to the $[NO(t)]$ theoretical curve given by the simulation and the F_X values have been determined previously.[9] Note that the NO^+ signal is corrected from the isotopic contribution of $^{13}C^{12}CH_5$. The simulations leading to the knowledge of the concentrations $[X(t)]$ presented in Figure 7 are performed using a simplified kinetic scheme which includes only one unknown parameter: $\sigma_{C_2H_5}^{ionVUV}$.

Let us first discuss the reactions presented in Table 1:

Since the disappearance of C_2H_5 may originate from the five reactions: (2) and (6)−(9) reported in Table 1, it is important to know in a first step the branching ratios of the reactions of C_2H_5 with NO_2 (reactions 2, 6, and 7), especially reaction 2 in order to simulate the kinetics of the system. Park and Gutman[36] have studied reaction 6 between 0.72 and 2.02 Torr. They found no pressure dependence and measured the product ratio $[C_2H_5O]/[C_2H_5NO_2]$ equal to 3.0 ± 0.6. As the $C_2H_5NO_2$ molecule is not detectable in the present study since its IE (10.92 eV)[32] is higher that the photon energies used in this work, we could not extract a branching ratio for reaction 6 of Table 1. However, we clearly identified the products C_2H_4 + HONO of reaction 7 by probing C_2H_4. Using the absolute photoionization cross section of C_2H_4 (2.1 Mb[4] at 10.54 eV) and the measured ratio $[C_2H_4]/[NO] = 0.18 \pm 0.06$, the branching ratio of reaction 7 is measured to be (12 ± 6)%. The large uncertainty of this branching ratio is related to the fact that the VUV photon energies used for the ionization are close to the IE of C_2H_4 and some internal energy may alter the photoionization cross section value at threshold. By using the ratio obtained by Park and Gutman[36] and our branching ratio for reaction 7, we conclude that the prominent reaction 2 has a branching ratio of (66 ± 12)%.

The other reactions of Table 1 which play a role in the kinetic simulations are the $C_2H_5 + C_2H_5$ reactions (reactions 8 and 9)

Table 1. Main Reaction Mechanisms Used in the Simulations of the Kinetics Fitted in Figure 7 for 1.6 Torr Total Pressure of He; Minor Cross Reactions Are Also Indicated, although They Are Not Included in the Kinetic Model (See the Text)

reaction	k_{298K} ($cm^3 \cdot molecule^{-1} \cdot s^{-1}$)	reference
	Main Reactions	
(2) $C_2H_5 + NO_2 \rightarrow C_2H_5O + NO$	$2.9\ (0.6) \times 10^{-11}$	Park and Gutman[36]
(6) $C_2H_5 + NO_2 \rightarrow C_2H_5NO_2$	$1.0\ (0.4) \times 10^{-11}$	Park and Gutman[36]
(7) $C_2H_5 + NO_2 \rightarrow C_2H_4 + HONO$	$0.5\ (0.2) \times 10^{-11}$	this work
(8) $C_2H_5 + C_2H_5 \rightarrow C_4H_{10}$	1.9×10^{-11}	Baulch et al.[25]
(9) $C_2H_5 + C_2H_5 \rightarrow C_2H_4 + C_2H_6$	2.3×10^{-12}	Baulch et al.[25]
	Minor Cross Reactions	
(10) $C_2H_5O + NO \rightarrow CH_3CHO + HNO$	1.3×10^{-11}	Atkinson et al.[47]
(11) $C_2H_5O + NO \rightarrow C_2H_5ONO$	1.1×10^{-11}	Atkinson et al.[47]
(12) $C_2H_5O + NO_2 \rightarrow C_2H_5ONO_2$	1.1×10^{-11}	DeMore et al.[48]
(13) $C_2H_5O + NO_2 \rightarrow CH_3CHO + HONO$	6.6×10^{-12}	Batt and Milne[49]

and the $C_2H_5O + NO$ reaction (reaction 10). The remaining secondary cross radical reaction 11 plays a very minor role here, less than 10%. Note at this point that the other secondary reactions 12 and 13 involving $C_2H_5O + NO_2$ do not play any role in the kinetic evolution of $C_2H_5^+$ or NO^+ and are not included in the kinetic simulation since they produce neither C_2H_5 nor NO.

Kinetics of the disappearance of C_2H_5 and the appearance of NO have been performed for various conditions (for example varying the C_2H_5 concentration in the $(2-10) \times 10^{12}$ molecule·cm^{-3} range), the only adjustable parameter being the photoionization cross section of the C_2H_5 radical relative to the photoionization cross section of NO. The kinetic fits used the rate constants of Table 1 and are presented in Figure 7. The simulation yields the ratio $\sigma_{C_2H_5}^{ion}/\sigma_{NO}^{ion} = (2.6 \pm 0.6)$ both at 10.48 and 10.54 eV. Using the absolute photoionization cross section of NO determined by Watanabe et al.,[37,38] $\sigma_{NO}^{ion} = (2.1 \pm 0.2)$ Mb at 10.48 and 10.54 eV, we obtain the same absolute photoionization cross section value for the ethyl radical at 10.48 and 10.54 eV: $\sigma_{C_2H_5}^{ion} = (5.6 \pm 1.5)$ Mb. The error bar (95% confidence interval) reflects not only the statistical uncertainty of the measurement but also the uncertainty on the branching ratio of reaction 2, the uncertainty on the absolute photoionization cross section of NO,[37,38] and finally the possible minor role of the C_2H_3 radical (see Discussion above). Considering the rather small exothermicity of the $C_2H_5 + NO_2 \rightarrow C_2H_5O + NO$ reaction ($\Delta H = -18.9$ kcal/mol $= -0.82$ eV[25]), we neglect the possible effect of the NO vibrational excitation on its absolute photoionization cross section.

To confirm the measured value of the photoionization cross section of C_2H_5, we performed a second experiment which was revealed to be slightly more accurate: it consists of measuring the ionization cross section of C_2H_5 relative to that of CH_3 at 10.54 eV by recording successively the CH_3 and C_2H_5 signals produced from the $CH_4 + F \rightarrow CH_3 + HF$ and $C_2H_6 + F \rightarrow C_2H_5 + HF$ reactions, respectively. The two reactions have an equivalent global first-order rate constant, with CH_4 or C_2H_6 concentrations in great excess compared to F concentration, which is the limiting parameter. The fluorine production being constant for more than 1 h, it has been found more reliable to measure the relative CH_3 and C_2H_5 concentrations successively several times rather than using a calibrated CH_4/C_2H_6 mixture which would lead to diffusion perturbation and uncertainties in the CH_4/C_2H_6 consumption. However it was checked that the use of the calibrated mixture gave similar results.

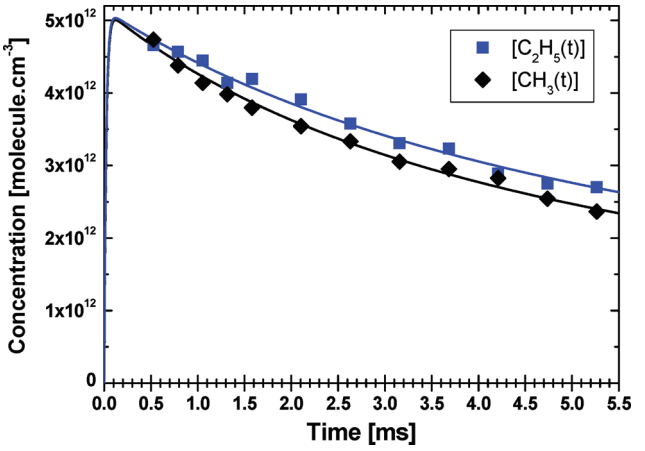

Figure 8. Typical kinetics of CH_3 and C_2H_5 with their respective simulations. Experimental points are shown by squares for $[C_2H_5(t)]$ and diamonds for $[CH_3(t)]$. The solid lines represent the simulations of C_2H_5 and CH_3 concentrations. To compare the kinetics of CH_3 and C_2H_5 radicals, the experimental C_2H_5 signal values are multiplied by $(\sigma_{CH_3}F_{CH_3})/(\sigma_{C_2H_5}F_{C_2H_5})$ relative to the CH_3 signal.

The apparatus function factor η of eq 5 is determined by fitting the CH_3^+ signal to the $[CH_3]$ theoretical curve given by the simulation. Taking into account the mass discrimination factors for CH_3 and C_2H_5 masses measured previously,[9] the only parameter to be determined is the ionization cross section of the ethyl radical. We modeled our experimental curve using a very simple kinetic scheme including only the reactions 1, 8, and 9 concerning C_2H_5 (with $k = 1.1 \times 10^{-10}$ $cm^3 \cdot molecule^{-1} \cdot s^{-1}$ for reaction 1[39]), and the following reactions for CH_3

$$CH_4 + F \rightarrow CH_3 + HF$$

$k = 6.4 \times 10^{-11}$ $cm^3 \cdot molecule^{-1} \cdot s^{-1}$ [40]

$$CH_3 + CH_3 \rightarrow C_2H_6$$

$k = 3.6 \times 10^{-11}$ $cm^3 \cdot molecule^{-1} \cdot s^{-1}$ [41]

The production of CH_3 and C_2H_5 radicals is achieved with CH_4 and C_2H_6 concentrations corresponding to equal global

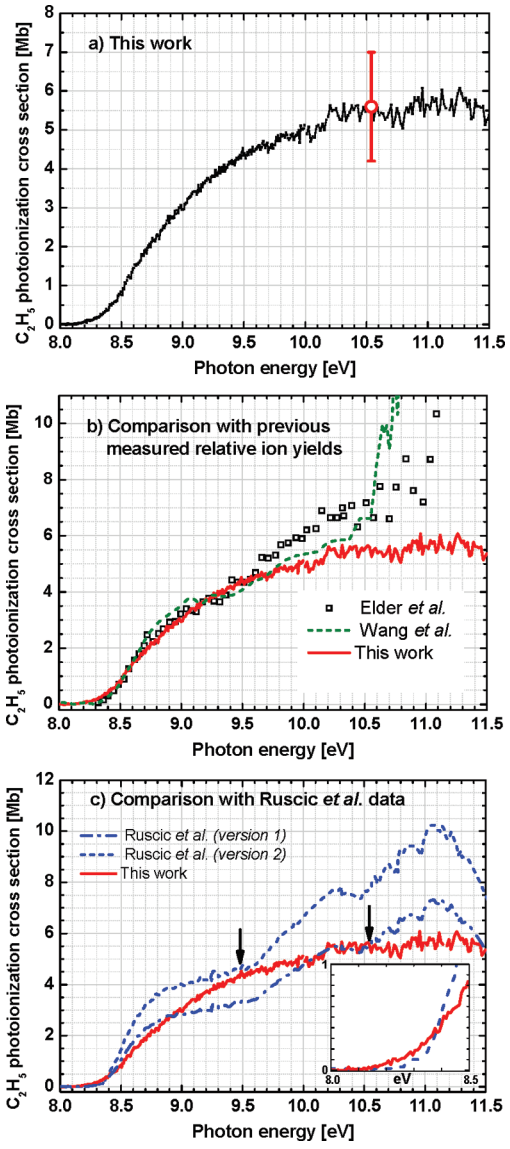

Figure 9. (panel a) Absolute photoionization cross section of C_2H_5 measured in this work from the synchrotron and the laser-based experiments between 8 and 11.5 eV. The red open circle corresponds to the absolute laser measurement, with its error bar, and is used to scale the whole synchrotron spectrum in absolute cross section units. (panel b) Comparison of the C_2H_5 photoionization cross section measured in this work with literature results plotted with an absolute scale: our results (red line), Wang et al.[5] (dotted green line), Elder et al.[14] (open black squares). (panel c) Comparison of the C_2H_5 photoionization cross section measured in this work (red line) with Ruscic et al.[1] within two alternative versions: version 1 (long-dashed blue line), version 2 (dashed-dotted blue line). The two arrows indicate the matching between our photoionization curve and Ruscic et al. curves in version 1 and version 2, respectively (see the text). The inset shows the adiabatic threshold region in an enlarged scale, with the same plot convention as for version 2.

first-order rate constants (typically 10000 s^{-1}) leading to a full consumption of fluorine atoms in less than 0.4 ms.

The result of our measurement is shown in Figure 8 and yields the photoionization cross section of the C_2H_5 radical relative to the photoionization cross section of CH_3. At 10.54 eV, we obtain $\sigma_{C_2H_5}^{ion}/\sigma_{CH_3}^{ion} = 1.10 \pm 0.12$, leading to $\sigma_{C_2H_5}^{ion\,10.54eV} = (5.6 \pm 1.4)$ Mb using the photoionization cross section of CH_3 determined in a previous study with the same apparatus[9] and considering the possible minor role of the C_2H_3 radical (see Discussion above).

C. Calibration of C_2H_5 Photoionization Curve and Comparison with Earlier Results. The direct total ion yield of C_2H_5 recorded at the synchrotron radiation facility (see Figure 5) can be rescaled on an absolute cross section scale using the laser measurements described in section B. We chose to use the value $\sigma_{C_2H_5}^{ion10.54eV} = (5.6 \pm 1.4)$ Mb, measured at 10.54 eV photon energy, since it carries the best accuracy in our study. The resulting absolute photoionization curve is displayed in Figure 9a. We can observe that at 10.54 eV our curve has reached a plateau for which the cross section becomes internal energy independent, as it was shown by Fan and Pratt.[19] This fully justifies that the absolute measurement performed on colder C_2H_5 radicals (see section III. B above) has been used for the calibration of our relative photoionization curve, as shown in Figure 9a.

At this point, it is interesting to compare our photoionization cross section with earlier C_2H_5 ionization data.[1,8,13,14,17,18] First of all, only one absolute value of the C_2H_5 photoionization cross section has been published so far at the fixed photon energy of 13.8 eV, that is 8 ± 2 Mb.[8] This value has been determined on ethyl radicals formed by photodissociation of ethyl chloride at 193 nm. The C_2H_5 photoionization cross section has been calibrated with respect to the absolute cross section of the Cl atom product.[42] In addition, the same authors tentatively proposed an estimate of this absolute cross section at 12.1 eV photoionization energy of about 16 Mb, which, according to the authors, should not be trusted to better than 50% due to the indirect measurement comparing the $C_2H_5^+$ counts at 13.8 and at 12.1 eV.[8] Although this photon energy is beyond the range of our cross section curve (see Figure 9a), the cross section value from ref 8 at 12.1 eV seems rather high, considering that our photoionization curve exhibits a flat profile above 10.5 eV and, at least, up to the maximum value of 11.5 eV. Therefore the very crude value proposed at 12.1 eV by FitzPatrick et al. is questionable. Nonetheless, the value of 8 Mb at 13.8 eV proposed by the same authors does not disagree with our cross section curve below 11.5 eV since new thresholds could appear in the ionization cross section of C_2H_5 and give rise to new increases of the cross section value. Excited triplet states of the cation have been characterized theoretically by Ruscic et al.[1] at 12.05 and 12.20 eV and probably more excited states lie in the 12−14 eV region.

The photoionization curves of the ethyl radical have been recorded previously in the literature via several types of radical production and are reported in panels b and c of Figure 9 with an absolute scale derived from Figure 9a for comparison with our data. Elder et al.[14] performed photoionization mass spectrometric studies of C_2H_5 using pyrolytic sources with three different precursors, $Pb(C_2H_5)_4$, $Hg(C_2H_5)_2$, and *sec*-butyl nitrite. Their results exhibit a very large dispersion in the photoionization curve shape depending on the precursor, so we have plotted in Figure 9b the results showing fewer fluctuations, related to the $Pb(C_2H_5)_4$ precursor molecule. Wang et al.[5] recorded an ion yield curve of C_2H_5 from a premixed gasoline/oxygen/argon flame between 8 and 11 eV (Figure 9b). A fair agreement is observed between our curve and those of Elder et al. and Wang et al. in the range 8−9.5 eV. Above 9.5 eV, the curves of refs 5 and 14 are affected by dissociative ionization processes and have not been corrected for them. The data obtained by Wang et al.[5] and Elder et al.,[14] performed with radicals formed in a flame and a pyrolysis source, respectively, are related to hot

C_2H_5 radicals albeit a little cooler than in our experiment if we compare the shape of the different curves between 8 and 9.5 eV in Figure 9b.

Ruscic et al.[1] used the same reaction F + C_2H_6 as the one described in section III.B, and performed a high-resolution photoion yield curve by using a many-line spectrum hydrogen lamp. Their results are plotted in Figure 9c with two possible absolute cross section scales (versions 1 and 2). Their spectrum exhibits a smooth steplike increase from the adiabatic ionization potential (8.117 eV) up to 11 eV with several oscillations (which were not observed in our experiment), and then it decreases up to 11.5 eV. In this discussion, we will disregard the portion of ion yield curve presented by these authors above 11.5 eV, since according to them, their spectrum has been affected by other contributions in the high-energy range.[1] The two alternative scalings used in version 1 and version 2 for the Ruscic et al. results are based on the following considerations: In version 1, the curve of Ruscic et al. is scaled by using our absolute value at 10.54 eV. At first sight, this version seems the most appropriate since C_2H_5 is produced by the same reaction in our laser experiment and in Ruscic experiment, although pressure and gas mixing conditions were different. Since our synchrotron experiment performed with a pyrolytic source produces hotter C_2H_5 radicals, at least with higher internal energy than the data presented by Ruscic et al.,[1] one could expect a discrepancy between our curve and that of Ruscic from the adiabatic threshold up to the plateau. From the PES spectrum obtained by Dyke et al. (see Figure 3 of ref 13) and from our SPES displayed in Figure 5, the photoionization curve is expected to reach a plateau corresponding to the sum of all Franck−Condon factors slightly above 9.5 eV, for the first ionization limit. This would imply that at around 9.5 eV our photoionization cross section and that of Ruscic et al. should match, which is not the case in version 1. That is why we tentatively propose to plot the Ruscic et al. curve as shown in version 2, for which both photoionization curves match at 9.5 eV. In version 2, the shapes of the curves are consistent with hot radicals in our case and cooler radicals in their case, as shown by the enlarged threshold region displayed in the inset of Figure 9c. In addition, a smoother increase of our cross section curve as compared to that of ref 1 is observed, leaving our curve below their curve between the adiabatic threshold and the first ionization plateau, as expected. In summary, between 8 and 9.5 eV, the version 2 plot of Ruscic et al. data seems more satisfactory than the version 1 plot. Unfortunately, a large discrepancy appears from about 9.5 eV with a second increase of the ionization curve of ref 1 up to 10.3 eV, followed by a decrease up to 10.5 eV and a new steplike increase up to 11 eV. Ruscic et al.[1] rationalized these oscillations by a tentative assignment to autoionizing Rydberg transitions converging toward the lowest $^3A''$ state predicted by theory at 12.05 eV. They based their assignment on the pertinent similarity between ionization of C_2H_6 from the uppermost occupied orbital[43] and ionization of C_2H_5 in the first excited triplet state of $C_2H_5^+$. They used the analysis of the absorption spectrum of C_2H_5 below the first ionization potential performed by Wendt and Hunziker[44] and, giving the quantum defects for 3s-like and 3p-like orbitals, they proposed to correlate: the first increase around 8.32 eV to the formation of a 3s-like state, the second increase at 9.54 eV to the formation of a 3p-like state, and the two other onsets at 10.46 and 10.75 eV to 4s-like and 4p-like states, respectively, with subsequent vibrational structures at higher energy. Ruscic et al.[1] also suggested that the lowest growth just above threshold could be attributed to changing Franck−Condon factors in the direct ionization yield, which seems to us more consistent with the comparison shown in the inset of Figure 9c. In the 9.5−11.5 eV energy range, our curve corrected from all possible contributions, in particular dissociative ionization above 10 eV, exhibits a flat profile, unlike the Ruscic et al. curve. At this stage, we do not understand this discrepancy since autoionizing features, if they have a significant strength as compared to direct ionization, should clearly appear in our synchrotron experiment (see for instance the photoionization spectrum of iodine we have recorded with the same apparatus, though at a better resolution in Figure 8 of ref 10). In addition, these autoionizing features would clearly occur in the photoelectron matrix used to create the SPES (see section III.A).

IV. CONCLUSION

This work presents the first measurement of the absolute photoionization cross section of the ethyl radical between the adiabatic threshold and 11.5 eV thanks to the synergy of two complementary measurements: one at fixed laser wavelengths and the other one performed with the tunable synchrotron light. A special care was taken in order to remove the contribution from dissociative ionization of the precursor by using an experimental discrimination based on the ion imaging technique. Note that most of the stable molecule precursors of this kind of radical exhibits relatively low dissociative ionization thresholds which may contaminate the photoionization curve. The ion imaging technique could then be a general method to extract direct ionization curves for many hydrocarbon radicals.

The C_2H_5 absolute photoionization cross section curve exhibits a plateau, roughly 2 eV above the adiabatic threshold and well below the second adiabatic threshold. The value at the plateau is expected to be the same whatever internal energy is deposited in the neutral radical[19] by a pyrolytic, photolytic, or reactive source. In order to check the shape of the ionization curve around threshold, it would be interesting to perform measurements on colder C_2H_5 radicals either by using a reactive production source with tunable VUV radiation or by using a pulsed pyrolytic source combined with a supersonic cooling, as described for instance by Weber et al.[45]

A new theoretical effort is needed to calculate the excited states of $C_2H_5^+$ cation in order to explain the increased ionization cross section found by FitzPatrick at 13.8 eV and to re-explore the region below 12 eV, for which an unexplained discrepancy is observed between the results of Ruscic et al.[1] and the present results. In the region around the first adiabatic threshold (8.117 eV), the vibrational frequencies of the ground state cation in its nonclassical C_{2v} geometry has been calculated by DeFrees and McLean.[46] Accurate calculations of higher excited vibrational structures and Franck−Condon factors between the neutral and cation ground states are highly needed in order to explain the experimental data in this threshold region, especially the still unassigned first ZEKE spectrum of Willitsch et al.[17] High-resolution threshold spectroscopy of the ethyl radical on a wider energy range would undoubtedly be of great interest, contributing to the assignment and extending the ZEKE spectrum to higher energies, albeit with a lower resolution.

■ ASSOCIATED CONTENT

Supporting Information. A table containing the absolute photoionization cross section of C_2H_5 in Mb as a function of

photon energy in eV, measured in the present work in the range (8−11.5 eV). This material is available free of charge via the Internet at http://pubs.acs.org.

AUTHOR INFORMATION

Corresponding Author

*E-mail: dolores.gauyacq@u-psud.fr; jc.loison@ism.u-bordeaux1.fr.

ACKNOWLEDGMENT

We acknowledge SOLEIL for provision of synchrotron radiation facilities and we are grateful to Dr. Christian Alcaraz for stimulating discussions.

REFERENCES

(1) Ruscic, B.; Berkowitz, J.; Curtiss, L. A.; Pople, J. A. *J. Chem. Phys.* **1989**, *91*, 114.
(2) Smith, D. *Chem. Rev.* **1992**, *92*, 1473.
(3) Herbst, E. *Chem. Soc. Rev.* **2001**, *30*, 168.
(4) Cool, T. A.; Wang, J.; Nakajima, K.; Taatjes, C. A.; McIlroy, A. *Int. J. Mass Spectrom.* **2005**, *247*, 18.
(5) Wang, J.; Wei, L.-X.; Yang, R.; Huang, C.-Q.; Shan, X.-B.; Sheng, L.-S.; Zhang, Y.-W.; Qi, F.; Yao, C.-D.; Li, Q.; Ji, Q. *Chem. Res. Chin. Univ.* **2006**, *22*, 375.
(6) Robinson, J. C.; Sveum, N. E.; Neumark, D. M. *J. Chem. Phys.* **2003**, *119*, 5311.
(7) Sveum, N. E.; Goncher, S. J.; Neumark, D. M. *Phys. Chem. Chem. Phys.* **2006**, *8*, 592.
(8) FitzPatrick, B. L.; Maienschein-Cline, M.; Butler, L. J.; Lee, S.-H.; Lin, J. J. *J. Phys. Chem. A* **2007**, *111*, 12417.
(9) Loison, J. C. *J. Phys. Chem. A* **2010**, *114*, 6515.
(10) Gans, B.; Vieira Mendes, L. A.; Boyé-Péronne, S.; Douin, S.; Garcia, G.; Soldi-Lose, H.; Cunha de Miranda, B. K.; Alcaraz, C.; Carrasco, N.; Pernot, P.; Gauyacq, D. *J. Phys. Chem. A* **2010**, *114*, 3237.
(11) Linstrom, P. J.; Mallard, W. G. *NIST Chemistry Web Book*; NIST Standard and Technology: Gaithersburg MD, 2001 (http:/webbook.nist.gov).
(12) Houle, F. A.; Beauchamp, J. L. *J. Am. Chem. Soc.* **1979**, *101*, 4067.
(13) Dyke, J. M.; Ellis, A. R.; Keddar, N.; Morris, A. *J. Phys. Chem.* **1984**, *88*, 2565.
(14) Elder, F. A.; Giese, C.; Steiner, B.; Inghram, M. *J. Chem. Phys.* **1962**, *36*, 3292.
(15) Quapp, W.; Heidrich, D. *J. Mol. Struct. (THEOCHEM)* **2002**, *585*, 105.
(16) Andrei, H.-S.; Solcà, N.; Dopfer, O. *Angew. Chem., Int. Ed.* **2008**, *47*, 395.
(17) Willitsch, S.; Wüest, A.; Merkt, F. *Chimia* **2004**, *58*, 281.
(18) Schussler, T.; Roth, W.; Gerber, T.; Alcaraz, C.; Fischer, I. *Phys. Chem. Chem. Phys.* **2005**, *7*, 819.
(19) Fan, H.; Pratt, S. T. *J. Chem. Phys.* **2005**, *123*, 204301.
(20) Garcia, G. A.; Soldi-Lose, H.; Nahon, L. *Rev. Sci. Instrum.* **2009**, *80*, 023102.
(21) DESIRS beamline, http://www.synchrotron-soleil.fr/portal/page/portal/Recherche/LignesLumiere/DESIRS.
(22) Mercier, B.; Compin, M.; Prevost, C.; Bellec, G.; Thissen, R.; Dutuit, O.; Nahon, L. *J. Vac. Sci. Technol., A* **2000**, *18*, 2533.
(23) Loison, J.-C.; Sanglar, S.; Villenave, E. *Rev. Sci. Instrum.* **2005**, *76*, 519.
(24) Zhou, J.; Lin, J. J.; Shiu, W.; Pu, S.-C.; Liu, K. *J. Chem. Phys.* **2003**, *119*, 2538.
(25) Baulch, D. L.; Bowman, C. T.; Cobos, C. J.; Cox, R. A.; Just, T.; Kerr, J. A.; Pilling, M. J.; Stocker, D.; Troe, J.; Tsang, W.; Walker, R. W.; Warnatz, J. *J. Phys. Chem. Ref. Data* **2005**, *34*, 757.
(26) Anderson, G. K.; Bauer, S. H. *J. Phys. Chem.* **1977**, *81*, 1146.
(27) DataBase, NIST, http://webbook.nist.gov/chemistry.
(28) Garcia, G. A.; Nahon, L.; Powis, I. *Rev. Sci. Instrum.* **2004**, *75*, 4989.
(29) Poully, J. C.; Schermann, J. P.; Nieuwjaer, N.; Lecomte, F.; Grégoire, G.; Desfrançois, C.; Garcia, G. A.; Nahon, L.; Nandi, D.; Poisson, L.; Hochlaf, M. *Phys. Chem. Chem. Phys.* **2010**, *12*, 3566.
(30) Ruscic, B.; Berkowitz, J. *J. Chem. Phys.* **1994**, *101*, 10936.
(31) Frost, M. J.; Smith, I. W. M. *J. Chem. Soc., Faraday Trans.* **1990**, *86*, 1751.
(32) Dewar, M. J. S.; Shanshal, M.; Worley, S. D. *J. Am. Chem. Soc.* **1969**, *91*, 3590.
(33) Uggerud, E. *Eur. Mass Spectrom.* **1997**, *3*, 403.
(34) del Rio, E.; Lopez, R.; Sordo, J. A. *J. Phys. Chem. A* **1998**, *102*, 6831.
(35) Bieri, G.; Niessen, W. V.; Asbrink, L.; Svensson, A. *Chem. Phys.* **1981**, *60*, 61.
(36) Park, J. Y.; Gutman, D. *J. Phys. Chem.* **1983**, *87*, 1844.
(37) Watanabe, K.; Matsugana, F. M.; Sakai, H. *Appl. Opt.* **1967**, *6*, 391.
(38) Watanabe, K.; Matsugana, F. M.; Sakai, H. *Appl. Opt.* **1967**, *6*, 1220.
(39) Persky, A. *Chem. Phys. Lett.* **2003**, *380*, 286.
(40) Atkinson, R.; Cox, R. A.; Crowley, J. N.; Hampson, R. F. IUPAC, http://www.iupac-kinetic.ch.cam.ac.uk, 2003.
(41) Wang, B.; Hou, H.; Yoder, L. M.; Muckerman, J. T.; Fockenberg, C. *J. Phys. Chem. A* **2003**, *107*, 11414.
(42) Berkowitz, J. *Atomic and Molecular Photoabsorption: Absolute Total Cross Sections*; Academic: San Diego, CA, 2002.
(43) *Higher Excited States of Polyatomic Molecules*; Robin, M., Ed.; Academic: New York, 1974; Vol. 1, pp120−129.
(44) Wendt, H. R.; Hunziker, H. E. *J. Chem. Phys.* **1984**, *81*, 717.
(45) Weber, K. H.; Lemieux, J. M.; Zhang, J. *J. Phys. Chem. A* **2009**, *113*, 583.
(46) DeFrees, D. J.; McLean, A. D. *J. Chem. Phys.* **1985**, *82*, 333.
(47) Atkinson, R.; Baulch, D. L.; Cox, R. A.; Hampson, J. R. F.; Kerr, J. A.; Rossi, M. J.; Troe, J. *J. Phys. Chem. Ref. Data* **1997**, *26*, 521.
(48) DeMore, W. B.; Sander, S. P.; Golden, D. M.; Hampson, R. F.; Kurylo, M. J.; Howard, C. J.; Ravishankara, A. R.; Kolb, C. E.; Molina, M. J. *JPL Publ.* **1997**, *4*, 1.
(49) Batt, L.; Milne, R. T. *Int. J. Chem. Kinet.* **1977**, *9*, 549.